Advancements in OCV Measurement and Analysis for Lithium-Ion Batteries

Mathias Petzl and Michael A. Danzer

***Abstract*—Incremental open-circuit voltage (OCV) curves and low-current charge/discharge voltage profiles of a lithium-ion (Li-ion) battery are compared and evaluated for optimizing measurement time and resolution. Since these curves are often used for further analysis, minimizing kinetic contributions is crucial for approximating battery OCV behavior. In this context, an incremental OCV measurement is characterized by state of charge (SOC) intervals and relaxation times. Various constant low C-rates, SOC intervals, and relaxation times are tested for approximating OCV behavior. Differential capacity and voltage analysis is used to check whether the main electrode features can be resolved satisfactorily. An interpolation method yields additional data points for the differential analysis of incremental OCV curves. It is shown that incremental OCV measurements are suitable for an approximation of battery OCV behavior, rather than low current–voltage profiles. Furthermore, extrapolation of voltage relaxation enables the estimation of fully relaxed OCV.**

***Index Terms*—Battery open-circuit voltage (OCV), extrapolation, interpolation, Li-ion, voltage relaxation.**

I. Introduction

STATE-of-the-art Li-ion batteries comprise high specific energy and constant performance, i.e., long cycle life. Various cell chemistries and cell types are available, due to the specific demands of battery applications like electric vehicles or consumer electronics.

In recent years, the olivine-type lithium iron phosphate ($LiFePO_4$) has proved to be a promising candidate for use as cathode active material [1], [2]. $LiFePO_4$ is beneficial in terms of power density, cycling, and thermal stability compared with common cathode materials (e.g., $LiCoO_2$). Disadvantages arise from the fact that $LiFePO_4$ exhibits a relatively low operating voltage which leads to decreased energy density.

The open-circuit voltage (OCV) is a very important characteristic of an electrode or battery cell. OCV curves display the electrodes' properties after the relaxation of kinetic processes, thus providing relevant thermodynamic information. As a special feature, $LiFePO_4$ shows an extremely flat OCV curve during lithium intercalation/deintercalation that proceed by a two-phase reaction [3]. In combination with inherent hysteretic behavior [4] and path dependence [5], state of charge (SOC) determination by simple OCV monitoring is very difficult. The OCV versus SOC relationship is crucial for battery modeling [6] and cell performance control in a battery management system [7]. In this context, electrochemical impedance spectroscopy has been discussed as an alternative technique for SOC estimation [8].

Here, we present a methodic study about different techniques for OCV measurements and possible optimizations. This aims to reduce or minimize kinetic contributions, i.e., polarization effects for the investigation of thermodynamic battery behavior. Usually, low-current charge/discharge voltage profiles are applied to approximate OCV curves. These will be compared with incremental OCV measurements, which consist of various SOC intervals and rest periods. Electrode features and their resolution are further investigated by analysis of differential capacity and differential voltage (DC/DV) [9]–[11]. An interpolation method is used to gain additional data points for OCV curves with large SOC intervals. It is shown that the number of measured data points can be significantly reduced with this method. Interpolation yields sufficient data points for detailed differential analyses. In general, long relaxation times are necessary for all electrode processes to relax. Thus, the relaxation of cell voltage is evaluated in terms of approaching OCV conditions. Extrapolation of relaxation behavior enables approximate estimation of fully relaxed state. This can be achieved by asymptotic fitting of relaxation characteristics. It is shown that extrapolated relaxation curves enable further reduction of measurement time by predicting the steady state of OCV. Finally, we will discuss which technique is suitable to investigate and approach battery OCV behavior, also regarding reduction of measurement time.

II. Experimental Details

The investigated cell is a cylindrical 26650-type Li-ion battery from a commercial vendor. This high power cell uses a $LiFePO_4$-based cathode in combination with graphite anode active material. The rated capacity is 2.5 Ah with cutoff voltages at 2.0–3.6 V (end of discharge voltage–end of charge voltage). All measurements are done on a BaSyTec CTS battery test system. To ensure constant temperature conditions of 25 °C, the cells are tested in an ESPEC climate chamber. Reproducibility is confirmed by investigation of three identical cells. Before each OCV measurement, the capacity is measured in order to exclude any severe cell aging effects. For the OCV investigation, we distinguish between incremental OCV curves

Manuscript received November 22, 2012; revised March 28, 2013; accepted April 14, 2013. Date of publication May 20, 2013; date of current version August 16, 2013. This work was supported by Helmholtz Institute Ulm Electrochemical Energy Storage and Zentrum für Sonnenenergie- und Wasserstoff-Forschung Baden-Württemberg. Paper no. TEC-00614-2012.

M. Petzl is with Helmholtz Institute Ulm Electrochemical Energy Storage, 89081 Ulm, Germany (e-mail: mathias.petzl@kit.edu).

M. A. Danzer is with Zentrum für Sonnenenergie- und Wasserstoff-Forschung Baden-Württemberg, 89081 Ulm, Germany and also with Helmholtz Institute Ulm Electrochemical Energy Storage, 89081 Ulm, Germany (e-mail: michael.danzer@zsw-bw.de).

Color versions of one or more of the figures in this paper are available online at http://ieeexplore.ieee.org.

Digital Object Identifier 10.1109/TEC.2013.2259490

and low-current charge/discharge voltage profiles. Incremental OCV measurements consist of SOC steps and relaxation periods. Here, SOC intervals (ΔSOC) of 0.5%, 1%, 5%, and various relaxation times, ranging from 6 min–5 h, are tested. Different SOC steps are attained by 1 C (2.5 A) constant current (CC) charging/discharging a certain amount of charge according to a particular interval. Afterward, the cell voltage is relaxed for a certain rest period to approximate OCV conditions. At the end of charge/discharge voltage, a constant voltage (CV) phase is applied until $|\mathrm{I}| < \mathrm{C}/40$ to ensure full charge/discharge of the cell before relaxation. Low-current charge/discharge voltage profiles consist of continuous constant current constant voltage (CCCV) measurements with various low C-rates (C/40, C/20, C/10, C/5, C/2). MATLAB is used for evaluation, analysis, and inter-/extrapolation of measurement data. A detailed description of the applied data interpolation and extrapolation methods is given in the next section.

III. Data Processing Methods

A. Interpolation

As discussed earlier, to reach the steady state of OCVs, long relaxation times are needed, leading to limited data points of OCV curves at finite measurement times. To get to a higher resolution of the OCV curve through data processing a monotone, nonlinear interpolation of OCV values is required. Therefore, we propose using piecewise cubic Hermite polynomials for the interpolation of OCV values, where OCV_k are the measured OCVs at the set SOC values SOC_k, with $k = 1, \ldots, N$. The first $N-1$ SOCs are set by a fixed amount of charge and hence are equally distributed. The last SOC is set via a cutoff voltage, where the amount of charge might differ to the other SOC intervals. $f_{\mathrm{int}}(\mathrm{SOC})$ is an underlying interpolating function at intermediate points, i.e., $f_{\mathrm{int}}(\mathrm{SOC}_j) = \mathrm{OCV}_j$. On each subinterval $\mathrm{SOC}_k \leq \mathrm{SOC} \leq \mathrm{SOC}_{k+1}$, $f_{\mathrm{int}}(\mathrm{SOC})$ is the cubic Hermite interpolant to the given values [12]. The slopes at the two endpoints are found such that the first derivative $df_{\mathrm{int}}(\mathrm{SOC})/d\mathrm{SOC}$ is continuous.

The interpolating function $f_{\mathrm{int}}(\mathrm{SOC})$ preserves the shape of the data, visually pleasing [13], and respects monotonicity. This means that, on intervals where the data are monotonic, so is $f_{\mathrm{int}}(\mathrm{SOC})$; and in general, at points where the data have a local extremum, so does $f_{\mathrm{int}}(\mathrm{SOC})$. In contrast to spline interpolation - where even the second derivative is continuous - $f_{\mathrm{int}}(\mathrm{SOC})$ has no overshoots and less oscillation if the data are not smooth.

B. Extrapolation

SOCs are set via CC charging or discharging of the cell. When the desired amount of charge is (re)moved, the current is switched off and the cell voltage is allowed to relax. Fig. 1(a) shows an equivalent circuit of the Li-ion cell with the terminal voltage and current, V_{cell} and I_{cell}, the frequency dependent, complex internal resistance, respectively, cell impedance Z_{cell}, and the OCV as voltage source. Due to the capacitive components in the impedance of the cell [see Fig. 1(b)], the cell voltage

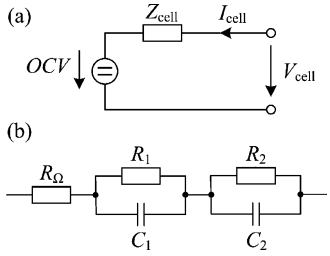

Fig. 1. (a) Equivalent circuit of a Li-ion cell with OCV, cell impedance Z_{cell}, terminal current I_{cell}, and terminal voltage V_{cell}. (b) Impedance model of a Li-ion cell with an ohmic resistance R_Ω and two *RC* circuits in series.

converges - after setting the current to 0—for $t \to \infty$ toward the OCV at the specific SOC.

Switching off the CC $I_{\mathrm{cell}} = I_{\mathrm{cc}}$ at $t = 0$ equals mathematically a step function $\sigma(t)$. The voltage as system response of the cell reacts with an instantaneous voltage step due to the ohmic resistance R_Ω and an exponential transient due to the *RC* circuits. The voltage at each *RC* circuit follows the equation $V_{RC} = R \cdot I_{\mathrm{cc}} \cdot \exp(-t/\tau)$ with the CC I_{cc} before the switch-off, the resistance R, and the time constant τ of the *RC* circuit. The time constant $\tau = R \cdot C$ is the product of the resistance and the capacitance of the *RC* circuit.

Hence, the modeled terminal voltage

$$V_{\mathrm{mod}} = R_\Omega \cdot I_{\mathrm{cc}} + \sum_i R_i \cdot I_{\mathrm{cc}} \cdot \exp(-t/\tau_i) + \mathrm{OCV} \quad (1)$$

is the sum of the ohmic voltage drop, the voltage drop at the *RC* circuits, and the OCV with the current I_{cc} as an input value and the unknown parameter vector

$$\boldsymbol{\theta} = [\mathrm{OCV}, R_\Omega, R_1, \tau_1, R_2, \tau_2, R_3, \tau_2]\,. \quad (2)$$

To identify the parameter vector θ of the model function, a nonlinear least-squares curve fitting problem of the form

$$\min_{\boldsymbol{\theta}} \|\mathbf{e}(\boldsymbol{\theta})\|_2^2 = \min_{\boldsymbol{\theta}} \left(e_1(\boldsymbol{\theta})^2 + e_2(\boldsymbol{\theta})^2 + \cdots + e_N(\boldsymbol{\theta})^2\right) \quad (3)$$

has to be solved. The used solver starts at the initial parameter vector $\boldsymbol{\theta}_0$ and finds a minimum of the sum of squares of the error function $e = V - V_{\mathrm{mod}}(I_{\mathrm{cc}}, \boldsymbol{\theta})$, where V are the measured voltage values of the relaxation. A set of lower and upper bounds is provided so that the solution is always in the range $\boldsymbol{\theta}_{\mathrm{lb}} \leq \boldsymbol{\theta} \leq \boldsymbol{\theta}_{\mathrm{ub}}$ and physically meaningless parameters such as negative resistances or time constants are avoided.

The optimization method used is a trust-region-reflective algorithm. This algorithm is a subspace trust-region method and is based on the interior-reflective Newton method [14], [15]. Each iteration involves the approximate solution of a large linear system using the method of preconditioned conjugate gradients.

IV. Results and Discussion

A. Resolution of Electrode Properties

Graphite and $\mathrm{LiFePO_4}$ have been studied intensively in terms of electrochemical behavior and phase transitions. The lithium intercalation/deintercalation of graphite proceeds via staging processes [16]–[19], i.e., different graphite-intercalation

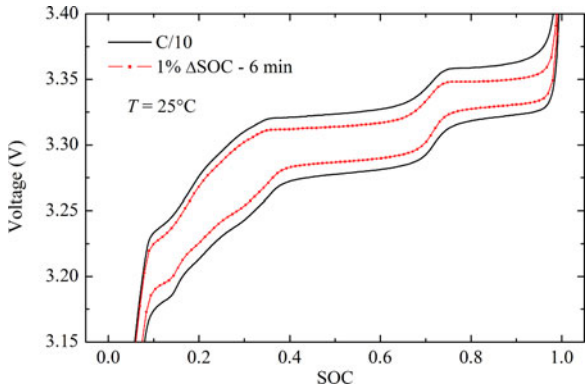

Fig. 2. C/10 low current–voltage profile (black) compared to incremental OCV curve with 1% SOC steps (ΔSOC) and 6 min relaxation periods (red).

compounds (GIC) Li_xC are gradually formed. On the contrary, $LiFePO_4$ exhibits only a single very flat plateau almost over the entire voltage profile. This is due to phase equilibrium during the topotactic lithium intercalation/deintercalation. In this context, a topotactic reaction is characterized by changes of atom positions.

Qualitatively, the three investigated cells show identical behavior. Representative results are shown here. Full cell voltage curves obviously provide the difference between electrode potentials. Fig. 2 depicts typical voltage profiles of the investigated battery, i.e., low current–voltage curve and incremental OCV measurement.

Two-phase regions (i.e., phase equilibria) are reflected as voltage plateaus, and voltage slopes indicate phase transitions according to Gibbs' phase rule. Due to the featureless $LiFePO_4$ voltage profile, the full cell exhibits only graphite characteristics, i.e., staging phenomena. Differential analysis of such curves enables detailed investigation of electrodes' phase behavior. Analysis of DC (dQ/dV versus V) translates voltage plateaus, i.e., phase equilibria into peaks, thus providing a better view on phase characteristics [9]. Usually, DC is used to investigate degradation effects (aging) of Lithium-ion batteries, e.g., loss of cyclable lithium or loss of active material [20]–[22]. Rate capability and polarization effects were also studied by DC in addition to simple capacity tests [23]. Phase transitions (single-phase regions) can be clarified by DV (dV/dQ versus Q) [24]. DV is especially useful if one of the electrodes does not show any features in the voltage profile [25]. In this case, a DV plot provides pure information about the graphite phase properties.

Thus, differential investigations have proved to be strong tools for nondestructive online characterization of Li-ion batteries. Corresponding DC and DV plots of the voltage profiles in Fig. 2 are shown in Fig. 3. The DC curves in Fig. 3(a) clearly illustrate the staging phase behavior of the graphite anode, with every peak characterizing a particular two-phase region. Height, shape, and position of the peaks allow for detailed analysis and comparison of electrode characteristics. Decreasing peak heights or peak shifts during cycling tests may indicate aging processes. Phase transitions are observable in a DV plot [see Fig. 3(b)] as peaks which arise from phase transitions at particular SOCs.

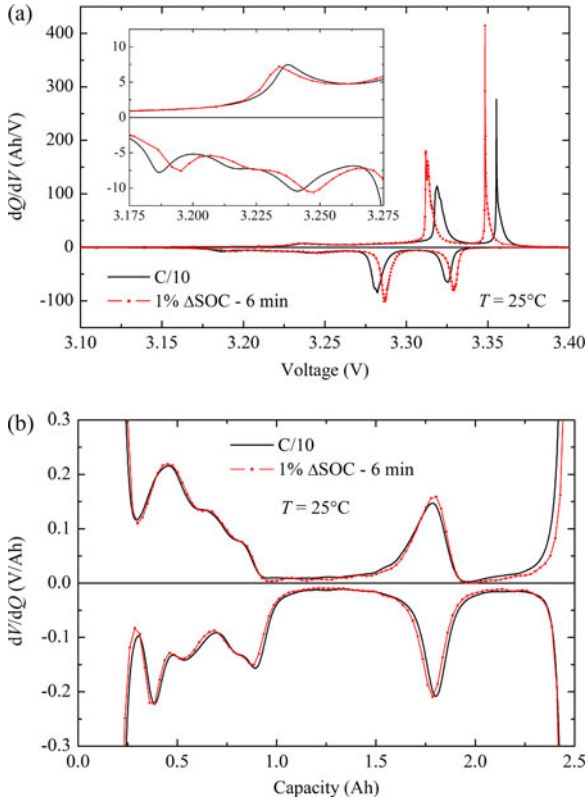

Fig. 3. (a) DC and (b) DV plots corresponding to Fig. 2.

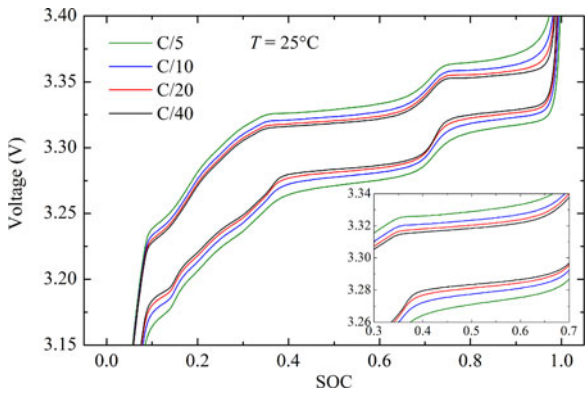

Fig. 4. Low-current charge/discharge profiles with C/40 (black), C/20 (red), C/10 (blue), and C/5 (green).

B. Measurement Techniques

This study does not focus on the well-known phase properties of graphite. Here, differential analysis is used to confirm if the electrode electrochemical characteristics can be resolved with different types of voltage, i.e., OCV measurements. A comparison of low-current charge and discharge voltage profiles with various C-rates is shown in Fig. 4. Increasing current leads to gradual losses of capacity due to polarization effects, as can be seen by vertical broadening of the voltage curves.

The hysteretic behavior is inherent and will not disappear even for infinitely small currents. But polarization can be decreased by lowering the applied C-rate. Differential analysis enables detailed investigation of these curves (see Fig. 5).

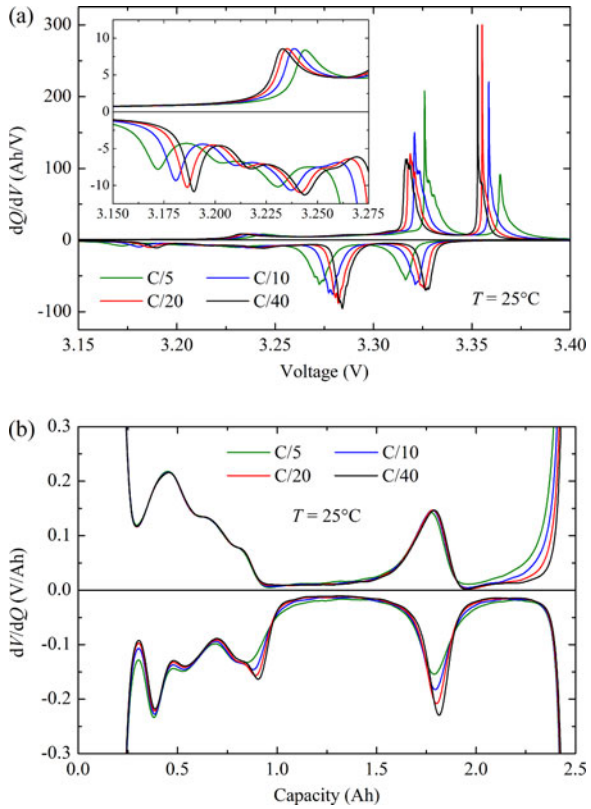

Fig. 5. (a) DC and (b) DV plots corresponding to Fig. 4.

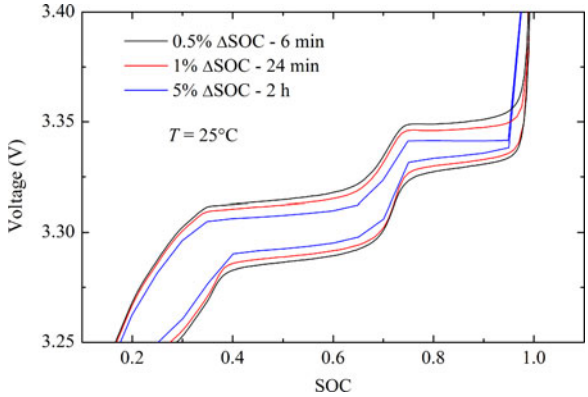

Fig. 6. Incremental OCV curves with different SOC intervals and rest periods: 0.5% ΔSOC-6 min (black), 1% ΔSOC - 24 min (red), 5% ΔSOC-2 h (blue).

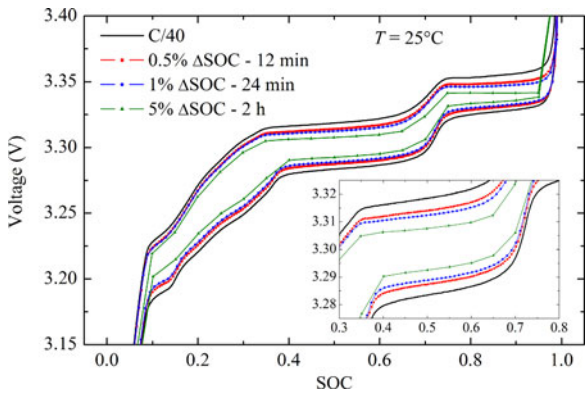

Fig. 7. Comparison of measurement techniques for identical measurement time (80 h): C/40 (black), 0.5% ΔSOC-12 min (red), 1% ΔSOC-24 min (blue), and 5% ΔSOC - 2 h (green).

Depending on the C-rate, the DC curves [see Fig. 5(a)] show strong differences as already qualitatively seen from the voltage profiles. DC now provides quantitative information about the electrochemical phase behavior. Clear trends for peak position and height are obvious in the discharge direction (i.e., negative *dQ/dV*). Peaks are shifted to lower potentials as the C-rate increases which is consistent with a lowering of the discharge voltage curve. Additionally, the peak heights decrease and peaks are broadened with rising current. The voltage profiles become steeper respectively. This is due to changes of (de)intercalation kinetics depending on the applied C-rate. Lithium ions are (de)intercalated faster as the current increases, thus altering the reaction characteristics. Peak broadening generally corresponds to deteriorated kinetics. Fig. 5(b) depicts the DV curves for various C-rates; all electrode features, i.e., phase transitions, are resolved satisfactorily. It is interesting to note that the phase transitions between lithium intercalated graphite stages (Li_xC) depend on the current differently. One would basically expect decreasing slopes (i.e., DV peaks) of the OCV curves in the phase transition region with growing C-rates. Three phase transitions are observed as one large DV peak with two small shoulders in the charge direction at low SOC, i.e., 0.3–0.9 Ah charge amount. These phase transitions exhibit no current dependence. The DV peak in the discharge direction at about 0.4 Ah grows with increasing C-rate, contrary to what is expected. Such phenomena are to be further investigated. Here, we apply differential analyses to see how the electrode phase behavior is resolved by different techniques.

Fig. 6 shows incremental OCV curves with various SOC steps (ΔSOC) and relaxation periods.

The question arises how to measure battery OCV behavior appropriately. Small SOC intervals provide more details and long relaxation periods reduce kinetic influences. Measurement time and resolution, i.e., detailedness, are critical factors in this context.

C. Identical Measurement Time

Assuming a measurement time of 80 h for a detailed OCV curve, there are several possibilities: either a low current–voltage profile with C/40 C-rate or incremental OCV measurements with various SOC intervals and relaxation periods (0.5% ΔSOC-12 min, 1% ΔSOC-24 min, 5% ΔSOC-2 h). Both techniques offer different advantages (see Fig. 7). Generally, it depends on the particular purpose which kind of measurement should be chosen. As can be seen from Fig. 7, even very small C-rates (C/40) cause polarization effects that are big enough to result in observable deviations from OCV behavior. For example, the potentials at 50% SOC differ about 10 mV (see inset of Fig. 7) depending on the applied technique (C/40 constant C-rate or 5% ΔSOC incremental OCV with 2 h relaxation periods).

Like aforementioned, both types of measurements can be suitable for a certain investigation. It is obvious that a low

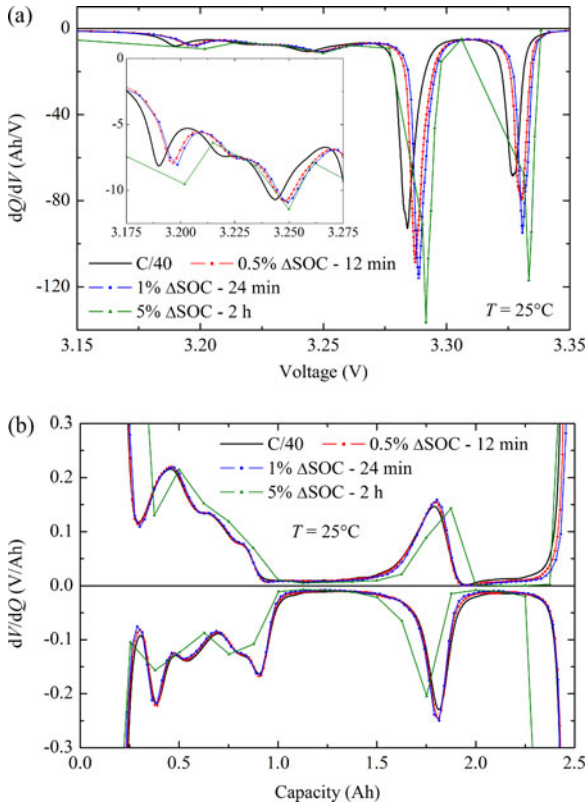

Fig. 8. (a) DC and (b) DV plots corresponding to Fig. 7; only the discharge direction is shown for DC.

current–voltage profile yields much more data points and thus higher resolution. Incremental OCV curves show minimized kinetic contributions due to relaxation at each SOC. For a more detailed comparison, Fig. 8 shows the corresponding DC and DV plots.

The DC curves [see Fig. 8(a)] clearly illustrate the excellent resolution of all electrode features (i.e., phase equilibria) for the constant C-rate voltage profile. A good resolution is also observed for the short SOC step (0.5%, 1%) incremental OCV curves.

As the rest periods increase, all DC peaks are shifted to higher potentials and the peaks grow in height. This is due to the decay of electrode polarization during relaxation and thus a decrease of kinetic contributions. Electrode processes relax and the potential increases/decreases (discharge/charge) until reaching fully relaxed state. As a consequence, the voltage plateaus are flattened and the DC peaks grow. Additionally, a higher charge amount can be discharged from the cell which means that the area of the corresponding DC peaks also increases. Thus, the two-phase regions are better utilized due to diminished polarization effects. Phase transitions are depicted by DV analysis [see Fig. 8(b)]. All electrode features can be resolved satisfactorily; only the 5% SOC steps cannot capture all properties of electrode phase behavior. DV peaks reflect the phase transitions between different graphite-intercalation compounds, i.e., staging processes. $LiFePO_4$ does not show any DV features due to a very flat voltage profile.

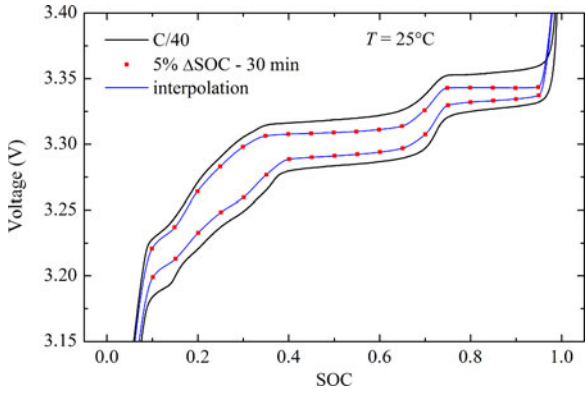

Fig. 9. Interpolation (blue) of incremental OCV data (red) with 5% SOC steps and 30 min relaxation periods. C/40 low current–voltage profile (black) is shown for comparison.

There is no measurement type suitable for all scopes, as can be seen from the aforementioned discussion; it depends on the aim of investigation. Incremental OCV curves also provide enough data points for detailed further analyses. SOC steps of 1%, i.e., 100 data points, seem to be sufficient for common OCV investigations; all features are resolved properly. On the contrary, low current–voltage profiles gain much more data points (depending on the registration). However, high numbers of data points ($\gg$1000) are not necessary to capture the electrode behavior comprehensively. Moreover, polarization effects are observed due to the constant low C-rate. This leads to the conclusion that incremental OCV measurements are generally more suitable for the investigation of battery OCV behavior.

D. Interpolation of OCV Data

Measurement time can be considerably reduced by larger SOC intervals (e.g., 5% ΔSOC). Thus, 20 data points are gained for a full charge or discharge which might be insufficient to reflect all electrode features. Interpolation is a common method to yield additional data. Here, we apply interpolation for better resolution and in consequence to reduce measurement time. Fig. 9 compares the C/40 low current–voltage profile with an interpolated 5% SOC step incremental OCV curve (relaxation: 30 min).

In this way, measurement time can be reduced by 75%. Interpolation provides enough data for detailed further analyses. Fig. 9 shows the measured open-circuit values and intermediate points calculated using the interpolating function $f_{\mathrm{int}}(\mathrm{SOC})$ with a resolution of 0.1% SOC. As desired, the shape and the monotonicity of the OCV values are preserved. Second, polarization effects are minimized due to voltage relaxation of the measured data points. Charge and discharge voltages are decreased and increased, respectively. This results in the reduction of hysteresis and the fully relaxed state is approximated. Advantages are even more obvious in the corresponding DC plot (see Fig. 10). In contrast to the measured OCV curve with a limited number of data points, the values of the interpolating function $f_{\mathrm{int}}(\mathrm{SOC})$ are well suited to calculate derivatives of the OCV curve as for the DC or DV analysis. As can be seen in Fig. 10,

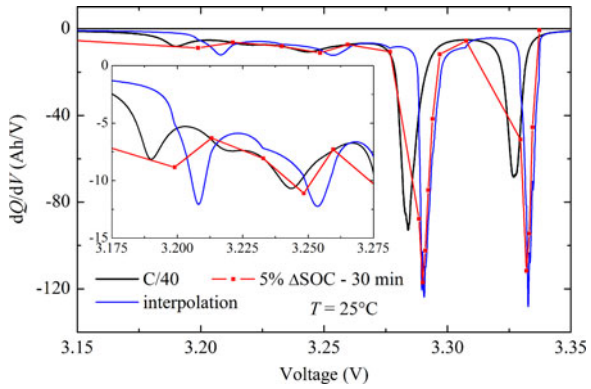

Fig. 10. DC plot corresponding to Fig. 9; only the discharge direction is shown.

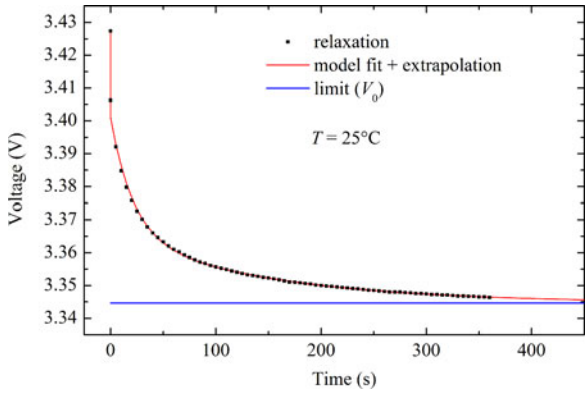

Fig. 11. Voltage relaxation for 6 min at 90% SOC after a CC charging period where the current is switched off at $t = 0$. Measured voltage values (black), the modeled voltage relaxation curve extrapolated beyond the last measured data point (red), and the asymptotic steady state ($t \rightarrow \infty$) OCV V_0 (blue).

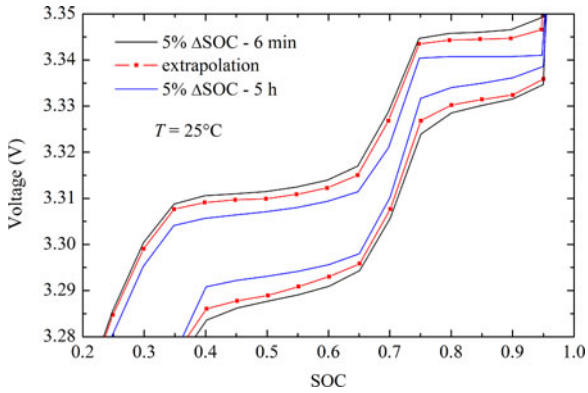

Fig. 12. Extrapolation (red) of an incremental OCV curve (black) compared to very long relaxation periods (blue).

the differential analysis of the interpolating function leads to the same features as continuous measurements do present. Even less pronounced features at low SOCs that would be lost without interpolation are reconstructed through the proposed data processing.

The DC curve of the original data exhibits poor resolution of phase properties, i.e., SOC intervals (5%) are too large. Small peaks at around 3.20 and 3.25 V are only characterized by a single data point. However, the most prominent features between 3.28 and 3.34 V are resolved satisfactorily. All peaks are shifted to higher potentials and increase in height compared with the C/40 DC curve. This is again due to the allowed relaxation of electrode processes. The benefit of interpolation is pointed out clearly by the respective DC curve. High resolution is attained for all peaks. Interpolation of OCV data (see Fig. 9) does not seem rewarding in the first place. But as can be seen from Fig. 10, the additional data points provide highly detailed differential analysis. Even the smaller peaks are well pronounced.

E. Extrapolation of Relaxation Behavior

Regarding incremental OCV measurements, relaxation of electrode processes, i.e., cell voltage is crucial for approximating steady-state conditions. Which relaxation time is appropriate for OCV measurements? There is no general answer to this question because electrode processes exhibit different time constants. Furthermore, relaxation behavior depends on the particular chemistry, temperature, and SOC. Relaxation of cell voltage can be fitted by an asymptotic function which implies a voltage limit V_0, i.e., steady-state conditions. Details of the applied extrapolation method were described previously. The relaxation behavior for a 5% ΔSOC incremental OCV measurement with 6 min relaxation time at 90% SOC is depicted in Fig. 11.

Voltage decreases due to the previous charging period to reach desired SOC. The fitted equivalent circuit model comprises two *RC* circuits (see Fig. 1), which characterize the main relaxation processes and their corresponding time constants. Fig. 11 shows the time series of the measured voltage relaxation in very good agreement with the modeled voltage relaxation function, leading to an error smaller than measurement accuracy. The asymptotic steady-state OCV V_0 for $t \rightarrow \infty$ can now be used instead of the last measured data point where the voltage is not yet fully relaxed. This enables the approximation of incremental voltage curves under fully relaxed conditions. In this way, measurement time can be further reduced because long relaxation periods are unnecessary. The proposed asymptotic fitting method provides a means to predict fully relaxed OCV by extrapolation of relaxation behavior.

Fig. 12 compares an incremental OCV curve (5% ΔSOC-6 min) with the corresponding relaxed data gained by extrapolation. A long relaxation (5 h) OCV measurement is shown for estimating the state of relaxation. As can be seen from Fig. 12, extrapolation allows for approaching the steady state; five hours of relaxation are assumed as fully relaxed conditions. The OCV extrapolation yields about 2 mV in voltage relaxation at each SOC in this case. However, fully relaxed cell voltage (5-h relaxation) is still 4 mV apart.

V. Conclusion

Low-current charge/discharge profiles provide high resolution of electrode features. But polarization effects are observable due to the applied CC. Thus, kinetic contributions cannot be neglected. Incremental OCV measurements yield less data points. However, 1% SOC intervals are sufficient for detailed

differential analyses, i.e., electrode phase properties are resolved satisfactorily. Significant reduction of kinetic contributions, i.e., polarization can be achieved with this method. Thus, incremental OCV measurements are more suitable for battery OCV approximation than low current–voltage profiles. This is due to the fact that only a limited amount of data points is needed for all electrode features to be resolved. Measurement time can be reduced by appropriate SOC steps and relaxation periods.

Interpolation of OCV data with large SOC steps is useful to increase detailedness and provides high resolution for further differential analysis. Less data points are thus needed for detailed OCV analyses and measurement time can be further reduced. Fully relaxed OCV, i.e., steady-state conditions can be estimated by asymptotic fitting of relaxation behavior and subsequent extrapolation. This enables approximation and prediction of fully relaxed state; rest periods are decreased significantly.

The presented OCV measurement techniques and data processing methods are suitable for all battery types, i.e., cell designs and chemistries.

REFERENCES

[1] A. K. Padhi, K. S. Nanjundaswamy, and J. B. Goodenough, "Phospho-olivines as positive-electrode materials for rechargeable lithium batteries," *J. Electrochem. Soc.*, vol. 144, pp. 1188–1194, 1997.

[2] M. Takahashi, S. Tobishima, K. Takei, and Y. Sakurai, "Reaction behavior of $LiFePO_4$ as a cathode material for rechargeable lithium batteries," *Solid State Ionics*, vol. 148, pp. 283–289, 2002.

[3] C. Delmas, M. Maccario, L. Croguennec, F. Le Cras, and F. Weill, "Lithium deintercalation in $LiFePO_4$ via a domino-cascade model," *Nature Mater.*, vol. 7, pp. 665–671, 2008.

[4] W. Dreyer, J. Jamnik, C. Guhlke, R. Huth, J. Moškon, and M. Gaberšček, "The thermodynamic origin of hysteresis in insertion batteries," *Nature Mater.*, vol. 9, pp. 448–453, 2010.

[5] V. Srinivasan and J. Newman, "Existence of path-dependence in the $LiFePO_4$ electrode," *Electrochem. Solid-State Lett.*, vol. 9, pp. A110–A114, 2006.

[6] M. A. Roscher and D. U. Sauer, "Dynamic electric behavior and open-circuit-voltage modeling of $LiFePO_4$-based lithium ion secondary batteries," *J. Power Sources*, vol. 196, pp. 331–336, 2011.

[7] S. Lee, J. Kim, J. Lee, and B. H. Cho, "State-of-charge and capacity estimation of lithium-ion battery using a new open-circuit voltage versus state-of-charge," *J. Power Sources*, vol. 185, pp. 1367–1373, 2008.

[8] S. Rodrigues, N. Munichandraiah, and A. K. Shukla, "A review of state-of-charge indication of batteries by means of a.c. impedance measurements," *J. Power Sources*, vol. 87, pp. 12–20, 2000.

[9] A. H. Thompson, "Electrochemical potential spectroscopy: A new electrochemical measurement," *J. Electrochem. Soc.*, vol. 126, pp. 608–616, 1979.

[10] M. Dubarry, V. Svoboda, R. Hwu, and B. Y. Liaw, "Incremental capacity analysis and close-to-equilibrium OCV measurements to quantify capacity fade in commercial rechargeable lithium batteries," *Electrochem. Solid-State Lett.*, vol. 9, pp. A454–A457, 2006.

[11] I. Bloom, A. N. Jansen, D. P. Araham, J. Knuth, S. A. Jones, V. S. Battaglia, and G. L. Henriksen, "Differential voltage analysis of high-power lithium-ion cells: 1. Technique and application," *J. Power Sources*, vol. 139, pp. 295–303, 2005.

[12] D. Kahaner, C. Moler, and S. Nash, *Numerical Methods and Software*. Englewood Cliffs, NJ, USA: Prentice-Hall, 1988.

[13] F. N. Fritsch and R. E. Carlson, "Monotone piecewise cubic interpolation," *SIAM J. Numer. Anal.*, vol. 17, pp. 238–246, 1980.

[14] T. F. Coleman and Y. Li, "An interior trust region approach for nonlinear minimization subject to bounds," *SIAM J. Optim.*, vol. 6, pp. 418–445, 1996.

[15] T. F. Coleman and Y. Li, "On the convergence of interior-reflective Newton methods for nonlinear minimization subject to bounds," *Math. Program.*, vol. 67, pp. 189–224, 1994.

[16] S. A. Safran, "Phase diagrams of staged intercalation compounds," *Phys. Rev. Lett.*, vol. 44, pp. 937–940, 1980.

[17] M. Noel and R. Santhanam, "Electrochemistry of graphite intercalation compounds," *J. Power Sources*, vol. 72, pp. 53–65, 1998.

[18] D. Aurbach, M. D. Levi, E. Levi, H. Teller, B. Markovsky, G. Salitra, U. Heider, and L. Heider, "Common electroanalytical behavior of Li intercalation processes into graphite and transition metal oxides," *J. Electrochem. Soc.*, vol. 145, pp. 3024–3034, 1998.

[19] D. Aurbach, B. Markovsky, I. Weissman, E. Levi, and Y. Ein-Eli, "On the correlation between surface chemistry and performance of graphite negative electrodes for Li ion batteries," *Electrochim. Acta*, vol. 45, pp. 67–86, 1999.

[20] M. Dubarry and B. Y. Liaw, "Identifying capacity fade mechanisms in a commercial $LiFePO_4$ cell," *J. Power Sources*, vol. 194, pp. 541–549, 2009.

[21] M. Safari and C. Delacourt, "Aging of a commercial graphite/$LiFePO_4$ cell," *J. Electrochem. Soc.*, vol. 158, pp. A1123–A1135, 2011.

[22] A. J. Smith, J. C. Burns, and J. R. Dahn, "High-precision differential capacity analysis of LiMn2O4/graphite cells," *Electrochem. Solid-State Lett.*, vol. 14, pp. A39–A41, 2011.

[23] M. Dubarry, C. Truchot, M. Cugnet, B.Y. Liaw, K. Gering, S. Sazhin, D. Jamison, and C. Michelbacher, "Evaluation of commercial lithium-ion cells based on composite positive electrode for plug-in hybrid electric vehicle application. Part I: Initial characterization," *J. Power Sources*, vol. 196, pp. 10328–10335, 2011.

[24] I. Bloom, J. Christophersen, and K. Gering, "Differential voltage analysis of high-power lithium-ion cells: 2. Applications," *J. Power Sources*, vol. 139, pp. 304–313, 2005.

[25] P. Liu, J. Wang, J. Hicks-Garner, E. Sherman, S. Soukiazian, M. Verbrugge, H. Tataria, J. Musser, and P. Finamore, "Aging mechanisms of $LiFePO_4$ batteries deduced by electrochemical and structural analyses," *J. Electrochem. Soc.*, vol. 157, pp. A499–A507, 2010.

Mathias Petzl was born in Göppingen, Germany, in 1985. He received the Diploma degree in chemistry from Ulm University, Ulm, Germany, in 2010. Since 2011, he has been working toward the Ph.D. degree with Helmholtz Institute Ulm Electrochemical Energy Storage, Ulm.

His research interests include the nondestructive characterization of Li-ion batteries, especially aging behavior and related degradation mechanisms.

Michael A. Danzer studied electrical and energy engineering at Ulm University, Ulm, Germany, and at Cardiff University, Cardiff, U.K. He received the Dipl.-Ing. and Dr.-Ing. (Ph.D.) degrees both in electrical engineering from Ulm University, Ulm, in 2003 and 2009, respectively.

His doctoral thesis was focused on the dynamics and efficiency of proton exchange membrane fuel cell systems. From 2009 to 2010, he was at A123 Systems, Inc., Boston, MA, USA, as a Research Scientist, where he was involved in research in the field of battery characterization and fundamentals of battery operation. Since 2011, he has been the Deputy Head of the Accumulator Department, Zentrum für Sonnenenergie- und Wasserstoff-Forschung Baden-Württemberg, Ulm, where he leads the Battery System Engineering Group. Since 2011, he has also been a Principal Investigator of the System Group, Helmholtz Institute Ulm Electrochemical Energy Storage, Ulm.